Chinese Chemical Letters 33 (2022) 2564–2568

Contents lists available at ScienceDirect

Chinese Chemical Letters

journal homepage: www.elsevier.com/locate/cclet

Efficiently photothermal conversion in a MnO_x-based monolithic photothermocatalyst for gaseous formaldehyde elimination

Pengfei Sun[1], Huijia Yu[1], Tingting Liu, Yingshuang Li, Zhongsen Wang, Yufei Xiao, Xiaoping Dong*

Department of Chemistry, Key Laboratory of Surface & Interface Science of Polymer Materials of Zhejiang Province, Zhejiang Sci-Tech University, Hangzhou 310018, China

ARTICLE INFO

Article history:
Received 9 August 2021
Revised 8 September 2021
Accepted 13 September 2021
Available online 20 September 2021

Keywords:
Photothermal catalytic
Melamine sponge
Graphene oxide
MnO_x
Formaldehyde

ABSTRACT

Volatile organic compound (VOC) pollution has a serious impact on human and urgently needs to be controlled through the development of new methods and catalytic materials. Compared with traditional thermal catalytic oxidation, the synergistic photothermocatalysis is regarded as a green and environmentally friendly strategy for organic compound pollutant removal, which can promote spontaneous heating of the surface of catalysts to achieve thermal catalytic reaction conditions *via* harvesting light irradiation. In this paper, a monolithic photothermocatalyst was synthesized through coating graphene oxide (GO) and MnOx in turn on a commercially available melamine sponge, where the GO mainly acted as a photothermal conversion layer to heat the catalytically active MnO_x. This monolithic catalyst presented excellent photo-induced activity for formaldehyde elimination under ambient conditions (~ 90% degradation ratio in 20 min for ~160 ppm initial concentration formaldehyde), and meanwhile possessed a high catalytic durability for multiple cycles. The kinetic study demonstrated that this photothermocatalytic process followed a pseudo-second-order kinetics. Finally, we proposed a possible formaldehyde degradation pathway based on *in situ* DRIFTS examination.

Recently, increasing attention has been focused on volatile organic compound (VOC) pollution, which can cause serious environmental pollution and human health problems [1]. Various strategies have been developed, but it still remains tremendous challenges to effectively and energy-saving eliminate VOCs. For example, traditional regenerative thermal oxidation (RTO) and regenerative catalytic oxidation (RCO) technologies need extra energy consumption to maintain the furnace temperature (generally > 500 °C) [2]. Other methods, including ultraviolet photocatalysis and biological methods, also require large amounts of electric energy to provide intensive ultraviolet light or drive massive biological reactors to achieve an ideal VOC removal efficiency [3–5]. Therefore, it is urgent to develop green and environmentally friendly approaches to meet the current global environmental theme of carbon neutrality and minimum carbon consumption.

The synergistic photothermocatalysis has been considered to be an efficient and low-carbon technology for removal of VOCs, in which the catalyst with photothermal property can be spontaneously self-heated under light illumination to drive thermocatalysis process [6]. Apparently, this photothermocatalysis possesses the advantages of both photocatalysis and thermocatalysis. It enables the catalyst to be activated by using of natural light source without extra energy consumption. However, the photothermal effect of transition metal oxide (TMO) catalysts mainly originates from the non-radiative recombination of electron-hole pairs produced by the *d-d* transition of metal ions upon the absorption of photons [7–9]. Because of the relatively large d-orbital splitting energy, TMOs can absorb UV-vis and partial infrared light, resulting in an inefficiently photothermal conversion [10,11]. To further improve the conversion from photo-energy to thermo-energy, black carbonaceous materials with superior photothermal property, like graphene or graphene oxide (GO), have been introduced [12,13]. Their good near-infrared absorption properties make the surface temperature rise quickly, enabling the modified TMOs to overcome the reaction energy barrier for typical VOC oxidation.

In this paper, we fabricated a monolithic catalyst through precipitating GO and MnO_x on a commercially available melamine sponge, and studied its photothermocatalytic activity for abatement of formaldehyde (HCHO) that is one of the most prevalent VOC pollutants, and its main source is its wide use in the spraying,

* Corresponding author.
E-mail address: xpdong@zstu.edu.cn (X. Dong).
[1] These authors contributed equally to this work.

https://doi.org/10.1016/j.cclet.2021.09.050
1001-8417/

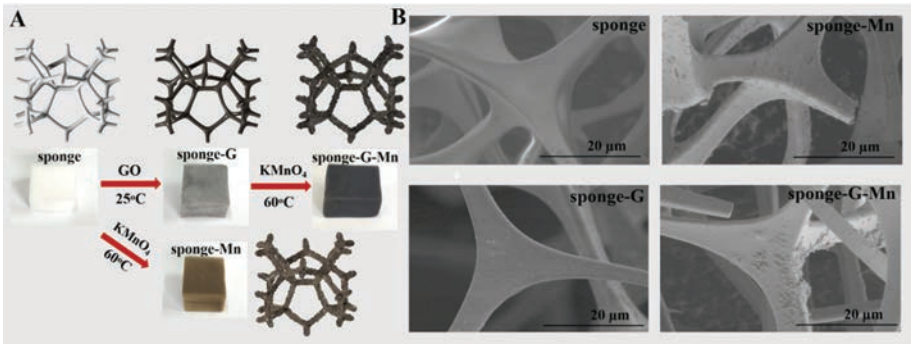

Fig. 1. Synthetic procedure (A) and SEM images (B) of sponge, sponge-Mn, sponge-G and sponge-G-Mn samples.

textile, wood processing and chemical production industries [14]. The developed three-dimensional (3D) porosity of sponge is favorable for mass transfer during the catalytic process and dispersing catalytic active materials to avoid their aggregation. Manganese oxide was selected as the active substance for HCHO oxidation due to its high concentration of oxygen vacancies and plentiful valence states, which endow it with excellent redox performance [15,16]. GO was used not only to convert photo-energy to thermo-energy, but also as a reductant medium to increase the loading of manganese oxide. We systematically characterized the physicochemical properties of this monolithic catalyst via different techniques and investigated its photothermocatalytic behaviors for HCHO degradation, including degradation efficiency, reaction kinetics, catalytic durability and photothermocatalytic mechanism.

The synthesis procedure of the monolithic catalyst was shown in Fig. 1A. Firstly, 0.16 g GO was dispersed in 20 mL of distilled water by sonication to form a homogeneous GO suspension. Then, a melamine sponge (white) with a size of 2.5 × 2.5 × 2.5 cm^3 was completely immersed into the GO suspension with the assistance of ultrasound treatment for 10 min. After that, the sponge was removed and dried naturally at room temperature, which was named as sponge-G (gray). This sponge-G was then immersed into the 0.025 mol/L $KMnO_4$ solution, after which it was heated at a temperature of 60 °C for 5 h. After being washed with distilled water and dried overnight, the monolithic sponge-G-Mn catalyst (black) was finally obtained. Similarly, the sponge-Mn sample (brown) was prepared via directly immersing a sponge without GO modification into $KMnO_4$ solution under other identical conditions. Potassium permanganate, graphene oxide (> 99.9%) were all supplied by Sinopham Chemical Reagent Co., Ltd. and used as obtained. Catalyst characterizations and photothermocatalytic tests were listed in Supporting information.

Fig. 1B exhibited the surface morphology evolution of melamine sponge after loading GO and MnO_x by the scanning electron microscope (SEM) technique. The pristine sponge possessed an interconnected porous network with a clean and smooth skeleton surface. No evident change was observed after coating GO on the sponge, which could be ascribed to the ultrathin 2D nanosheet-like morphology of GO and its homogeneous cover. Through redox reaction between $KMnO_4$ and the sponge-G or the pristine sponge, it was clearly found that the surface of sponge became rough due to the MnO_x precipitation. Compared to the sponge-Mn, more MnO_x particles were modified on the surface of the sponge-G-Mn sample. This result demonstrated that the GO layer was benefit to the MnO_x loading.

Energy dispersive X-ray spectroscopy (EDS) was employed to further prove the formation of the sponge-G-Mn structure (Fig. 2A). Five elements, C, N, K, Mn and O were checked, and their distributions in elemental mappings were highly uniform, suggesting GO and MnOx were successfully loaded on the sponge skeleton. Fig. 2B shows the XRD patterns of different sponge samples. The characteristic peak at approximately 10° was ascribed to graphene oxide [17], which was observed on the sponge-G and sponge-G-Mn samples. For the sponge-G-Mn sample, another two diffractions at the 2θ values of 36.5° and 65.5° were indexed to the (100) and (110) planes of an Akhtenskite MnO_x phase (JCPDS No. 30-0820). However, these characteristic peaks became indistinct in the sponge-Mn sample, which might be due to the low loading content. The weight percent of Mn is 12.403% and 1.2838% for catalyst sponge-G-Mn and sponge-Mn tested by inductively coupled plasma atomic emission spectrometry (ICP-AES). The transmission electron microscopy (TEM) image of surface particles on the sponge-G-Mn sample (Fig. 2C) also demonstrated a d-spacing of 0.45 nm, matching the interlayer distance of the (100) facet of the MnOx crystal [18,19].

X-ray photoelectron spectroscopy (XPS) was used to analyze the state of the surface elements (Fig. 3). The C 1s spectra of the sponge-G, sponge-Mn and sponge-G-Mn samples (Figs. 3A-C) presented four main components at 284.7, 286.9, 287.7 and 288.9 eV, which were assigned to C-C/C=C (unoxidized, aromatic sp2 structures), C-O (epoxy and alkoxy), C=O (carbonyl) and O-C=O (carboxyl) groups [20], respectively. Compared to the sponge-G, the proportions of oxygen-containing species in the sponge-G-Mn sample decreased dramatically, indicating that MnOx was produced from the redox reaction between $KMnO_4$ and these oxygen-containing groups on GO [21,22]. Considering the absence of GO in the sponge-Mn, the oxygen-containing species should originate from the oxidation of sponge skeleton by $KMnO_4$. In addition, the O-C=O peak in the sponge-Mn shifted to lower binding energy than those in other two sponge samples. It could be ascribed to the exposed sponge framework without GO coating, where the carbon atom in C-N conjugated skeleton has a binding energy of 288.4 eV [23]. Two characteristic peaks with a splitting energy of 11.6 eV were revealed in the Mn 2p spectra (Fig. 3D), which were respectively assigned to Mn $2p_{3/2}$ (641.8 eV) and Mn $2p_{1/2}$ (653.4 eV), well agreeing with that of tetravalent Mn ion in MnO_2 [24,25]. The deconvoluted O 1s spectra of the sponge-G, sponge-Mn and sponge-G-Mn samples (Fig. 3E) displayed three peaks at 529.6, 531.2 and 532.6 eV, which could be indexed to lattice oxygen (O_{lat}, Mn-O-Mn) [21,26], surface oxygen (O_{suf}, Mn-OH) [27,28] and C–O/C=O groups [21], respectively. The sponge-G-Mn had a much higher O_{lat} proportion than the sponge-Mn, implying that much more MnO_x was modified on the sponge [25,29]. In addition, an electron spin resonance (ESR) experiment (Fig. S1 in Supporting information) also confirmed the presence of a large number of oxygen vacancies on the surface of sponge-G-Mn, which is caused by the massive formation of MnO_x on GO surface.

Photothermocatalytic activity of these monolithic sponge catalysts were evaluated by degrading HCHO (~160 ppm) under ambient temperature using 300 W xenon light. As shown in Fig. 4A, the

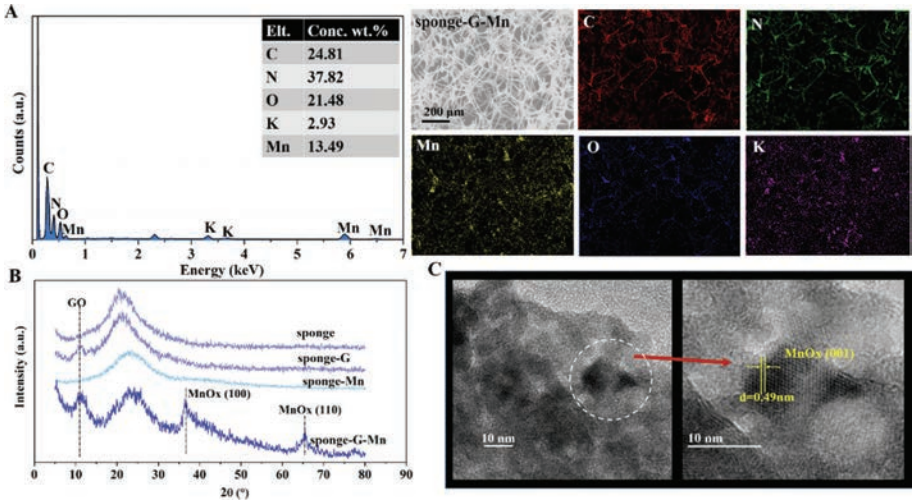

Fig. 2. (A) EDS-mapping test of sponge-G-Mn sample. (B) XRD patterns of sponge, sponge-G, sponge-Mn and sponge-G-Mn samples. (C) HR-TEM images of sponge-G-Mn sample.

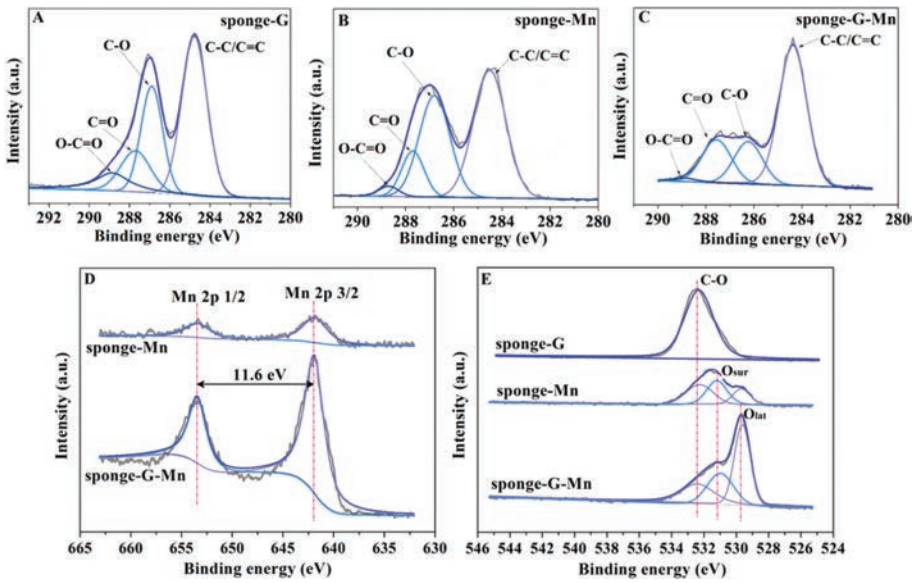

Fig. 3. XPS spectra of the C 1s spectra of (A) sponge-G, (B) sponge-Mn, (C) sponge-G-Mn. (D) The Mn 2p spectra of sponge-Mn and sponge-G-Mn. (E) The O 1s spectra of sponge-G, sponge-Mn, sponge-G-Mn.

HCHO concentration did not obviously change in the blank experiment (without catalyst), indicating the photo-stability of HCHO. For the sponge and sponge-G samples, a slight decrease in HCHO concentration resulted from physical adsorption. The sponge-Mn sample exhibited a degree of HCHO removal performance due to the surface MnO_x. HCHO oxidation over TMO catalysts is well known to follow a metal-assisted Mars-van Krevelen (MvK) mechanism, in which the surface OH^- groups and lattice oxygen concentrations act as main factors for determining catalyst performance [30,31]. However, the relatively weak photothermal conversion of MnO_x induced a low surface temperature of catalyst and then suppressed the activation of surface lattice oxygen. After inducing the GO layer onto the sponge skeleton, the surface temperature of catalyst would be significantly improved due to the well photothermal conversion ability of GO, therefore promoting the surface oxygen activation on MnOx. Thus, an excellent performance of HCHO removal was observed on the sponge-G-Mn sample, the HCHO concentration decreasing rapidly during the first 5 min and ultimately stabilizing at approximately 90%. Fig. 4B displayed the influence of irradiations with different wavelength ranges on the HCHO conversion on the sponge-G-Mn catalyst. The HCHO removal ratio in the absence of light illumination was similar to the adsorption effect of the sponge and sponge-G sample, indicating the sponge-G-Mn sample had little activity for HCHO oxidation without light. The slight increase of the HCHO removal ratio under UV-vis should be attributed to the weak photocatalytic activity of MnO_x. With presence of near infrared (NIR) light, the elimination efficiency was greatly improved, and under UV-vis-NIR illumination the sponge-G-Mn presented the best catalytic activity, which provided a possibility for utilization of the whole sunlight spectrum to purify air.

To reveal the origin of catalytic activity enhancement under light irradiation, we studied the optical properties of these sponge catalysts (Fig. 4C). Due to the presence of GO, the sponge-G-Mn catalyst possessed intensive absorption in the whole spectral region, as shown in the UV-vis-NIR diffuse-reflectance spectrum (DRS). This result was consistent with the rising tendency of sur-

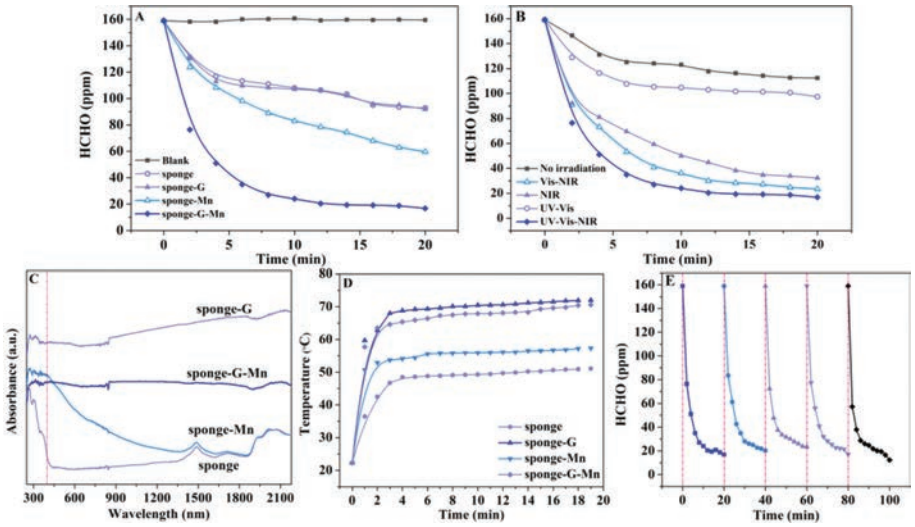

Fig. 4. (A) Catalytic performance of modified sponge catalysts for HCHO elimination under xenon light irradiation. (B) Catalytic performance of sponge-G-Mn catalyst for HCHO elimination under irradiation with different wavelength ranges. (C) UV–vis-NIR DRS profiles of sponge, sponge-G, sponge-Mn, sponge-G-Mn samples. (D) Degrees of catalyst surface temperature increase for sponge, sponge-G, sponge-Mn, sponge-G-Mn samples. (E) Reusability testing for the sponge-G-Mn catalyst.

Table 1
Apparent rate constants of HCHO degradation from *pseudo*-first-order and *pseudo*-second-order models.

Sample	*Pseudo*-first-order kinetics		*Pseudo*-second-order kinetics	
	k_1 (min^{-1})	R^2	k_2 (ppm^{-1} min^{-1})	R^2
Sponge	2.93×10^{-2}	0.7878	2.33×10^{-4}	0.8259
Sponge-G	2.94×10^{-2}	0.7223	2.34×10^{-4}	0.7531
Sponge-Mn	5.57×10^{-2}	0.9387	5.24×10^{-4}	0.9791
Sponge-G-Mn	1.63×10^{-1}	0.9191	3.61×10^{-3}	0.9956

face temperature (Fig. 4D). After illumination with xenon light for 18 min, the surface temperature of the sponge-G-Mn was rapidly increased to ~70 °C similar to the sponge-G sample, much higher than those of the bare sponge and the sponge-Mn. This result indicated the temperature enhancement was mainly contributed from the NIR absorption by the GO layer [32]. The significantly increased surface temperature by absorption of NIR undoubtedly promoted the activation of MnOx to improve the HCHO oxidation.

Fig. 4E depicted the recycling experiment results of the sponge-G-Mn catalyst to verify a practical performance for HCHO removal. For five successive runs, the HCHO degradation efficiency in every test was almost the same as that in the first test, which suggested that this sponge-G-Mn catalyst had a superior catalytic durability for HCHO removal under light irradiation. The XRD parttens also exhibited that there was no significant difference between the used sponge-G-Mn and brand new sponge-G-Mn (Fig. S2 in Supporting information).

The kinetics of the photothermocatalytic process were investigated using the *pseudo*-first-order (Eq. 1) and *pseudo*-second-order (Eq. 2) models [5]:

$$\ln(C/C_0) = -k_1 t \quad (1)$$

$$(1/C) - (1/C_0) = k_2 t \quad (2)$$

In these formulas, t is the irradiation time, C_0 and C represent the initial HCHO concentration and the HCHO concentration after t min of irradiation, respectively, and k_1 and k_2 are the apparent rate constants of *pseudo*-first-order kinetics and *pseudo*-second-order kinetics, respectively. As shown in Fig. S3 (Supporting information) and Table 1, the correlation coefficient (R^2) indicates that the *pseudo*-second-level model is more suitable for describing the catalytic process of HCHO removal than the *pseudo*-first-level model. The calculated k_2 value of sponge-G-Mn was 3.61×10^{-3} ppm^{-1} min^{-1}, which was 6.90, 15.43 and 15.49 times higher than those of sponge-Mn, sponge-G and sponge, respectively. This kinetic constant value exceeded those of the traditional indoor TiO_2 photocatalysts such as rGO/TiO_2 [33] and Fe/TiO_2 [34] reported in the literatures, indicating the excellent formaldehyde removal performance of the sponge-G-Mn catalyst.

To study the mechanism of the photothermocatalytic oxidation of HCHO over sponge-G-Mn catalysts, *in situ* DRIFTS with light illumination was conducted. Fig. 5 illustrated several characteristic peaks at 1456, 1508, 1520, 1623, 2336, 2365 and 3634 cm^{-1}. Among them, the absorptions at 1456 and 1520 cm^{-1} were respectively related to the stretching vibrations of dioxymethylene (DOM) and formate ($HCOO^-$) species, both of which were main intermediates during the HCHO oxidation process [35,36]. The peaks at 1508 and 1623 cm^{-1} were ascribed to carbonate species, in accordance with the peaks at 2336 and 2365 cm^{-1} that belonged to CO_2, confirming that $HCOO^-$ was further oxidized into carbonate and CO_2 [30,37]. With the prolongation of reaction time, the intensity of these vibration peaks increased gradually, indicating that the oxidation HCHO became gradually intense. Meanwhile, a negative band at 3634 cm^{-1} resulted from the consumption of surface metal-OH groups [38,39], suggesting that Mn-OH participated in the reaction as an adsorption site of HCHO molecule through hydrogen bonding.

Finally, a plausible mechanism for HCHO oxidation over sponge-G-Mn was proposed. The surface MnOx loaded on the sponge could oxidize HCHO at room temperature, but the oxidation efficiency was limited due to the lack of external energy input. However, the surface temperature would quickly increase because of the effective near-infrared absorption of GO, which ultimately activated surface lattice oxygen (Mn-O) to induce the MvK mechanism for HCHO oxidation [40]. As revealed in Fig. 5, HCHO molecules (reactants) were firstly adsorbed onto -OH groups through hydrogen bonding. After that, the lattice oxygen formed by the activation of the M-O bond attacked the adjacent electrophilic C atoms of the adsorbed HCHO molecule, thereby producing DOM intermediates, which were rapidly oxidized and converted into formates (intermediates) [41]. These intermediate products would be further oxidized to CO_2 and H_2O. The consumed lattice oxygen would

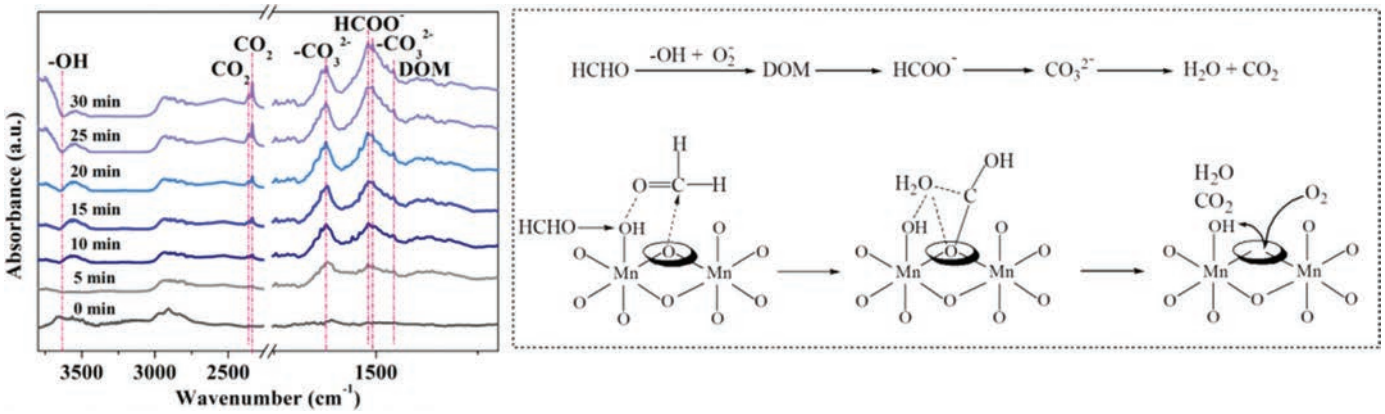

Fig. 5. In situ DRIFTS of the HCHO reaction on the sponge-G-Mn catalyst under xenon light irradiation and reaction mechanism of formaldehyde.

form oxygen vacancies, which could be replenished by dioxygen molecules in air and maintain catalyst reusability.

In summary, this monolithic sponge-G-Mn catalyst was successfully synthesized by a facile *in situ* growth method and exhibited excellent HCHO removal efficiency at room temperature with assistance of light irradiation. With the addition of GO, the loading capacity of MnOx on the skeleton of sponge was significantly increased, which endowed this common melamine sponge with good indoor HCHO removal properties. Furthermore, the absorption of NIR light by GO promoted the increase of surface temperature and induced an MvK mechanism on MnOx for HCHO oxidation. The monolithic catalyst could efficiently eliminate HCHO and meanwhile possessed a high catalytic durability for long-time use. The *in situ* DRIFTS experiments showed that HCHO was firstly oxidized to DOM and formate and was eventually oxidized to CO_2 and H_2O as the reaction continues. This sponge-G-Mn composite can act as a cost-effective catalyst for formaldehyde oxidation and has huge application prospects in other gaseous pollutant removal reactions.

Declaration of competing interest

The authors declare that they have no known competing financial interests or personal relationships that could have appeared to influence the work reported in this paper.

Acknowledgments

This work was financially supported from the National Key Research and Development Program of China (No. 2017YFE0127400), the Natural Science Founding of China (No. 51908491), the Zhejiang Provincial Natural Science Foundation of China (No. LY20B070001), and Science Fund of Zhejiang Sci-Tech University (No. 21062255-Y).

Supplementary materials

Supplementary material associated with this article can be found, in the online version, at doi:10.1016/j.cclet.2021.09.050.

References

[1] Q. Zhang, M. Shao, Y. Li, et al., Chin. Chem. Lett. 23 (2012) 1059–1062.
[2] J.J. Liu, X.X. Dai, Z.B. Wu, X.L. Weng, Chin. Chem. Lett. 31 (2020) 1410–1414.
[3] P. Qiu, T. Zhao, X. Zhu, et al., Chin. Chem. Lett. 32 (2021) 1456–1461.
[4] R. Wang, C. He, W. Chen, C. Zhao, J. Huo, Chin. Chem. Lett. 32 (2021) 3821–3824.
[5] Y.J. Chen, S.F. Ji, W.M. Sun, et al., Angew. Chem. Int. Ed. 59 (2020) 1295–1301.
[6] Z. Wang, H. Yu, Y. Xiao, et al., J. Hazardous Mater. 407 (2021) 124795.
[7] Z. Wang, H. Yu, L. Zhang, L. Guo, X. Dong, J. Taiwan Institute Chem. Engin. 107 (2020) 119–128.
[8] Y. Yang, Y. Li, M. Mao, M. Zeng, X. Zhao, ACS Appl. Mater. Interf. 9 (2017) 2350–2357.
[9] X. Lian, Z. Jian, Q. Li, et al., Appl. Surf. Sci. (2021) 149207.
[10] S. Peng, X. Yang, J. Strong, et al., J. Hazardous Mater. 396 (2020) 122750.
[11] J. Wang, G. Zhang, P. Zhang, Appl. Catal. B: Environ. 239 (2018) 77–85.
[12] Q. Zhang, W. Xu, X. Wang, Sci. China Mater. 61 (2018) 905–914.
[13] L. Fu, R. Wang, C. Zhao, et al., Chem. Engin. J. 414 (2021) 128857.
[14] G. Liu, J. Zhou, W. Zhao, Z. Ao, T. An, Chin. Chem. Lett. 31 (2020) 1966–1969.
[15] P. Wu, S.Q. Dai, G.X. Chen, et al., Appl. Catal. B: Environ. 268 (2020) 118418.
[16] Z.H. Xu, N.H. Wang, Z.X. Yan, et al., Appl. Surf. Sci. 510 (2020) 145500.
[17] S.H. Aboutalebi, A.T. Chidembo, M. Salari, et al., Energy Environ. Sci. 4 (2011) 1855–1865.
[18] J. Ye, M. Zhou, Y. Le, B. Cheng, J. Yu, Appl. Catal. B: Environ. 267 (2020) 118689.
[19] Y. Yang, Y.Z. Li, Q. Zhang, et al., J. Mater. Chem. A 6 (2018) 14195–14206.
[20] J. Zhang, H. Yang, G. Shen, et al., Chem. Commun. 46 (2010) 1112–1114.
[21] Q. Zhao, D. Chen, Y. Li, et al., Nanoscale 5 (2013) 882–885.
[22] Z. Hu, Y. Zhao, J. Liu, et al., J. Colloid Interf. Sci. 483 (2016) 26–33.
[23] W. Zhou, G. Li, L. Wang, Z. Chen, Y. Lin, Appl. Surf. Sci. 413 (2017) 140–148.
[24] J. Qu, L. Shi, C. He, et al., Carbon 66 (2014) 485–492.
[25] L. Lu, H. Tian, J. He, Q. Yang, J. Phys. Chem. C 120 (2016) 23660–23668.
[26] Q. Li, Y. Wang, J. Zeng, et al., Chin. Chem. Lett. 32 (2021) 3355–3358.
[27] W. Hu, X. Gao, Y. Deng, et al., Chem. Engin. J. 293 (2016) 118–128.
[28] N. Russo, D. Fino, G. Saracco, V. Specchia, J. Catal. 229 (2005) 459–469.
[29] Z. Wang, H. Yu, Y. Xiao, et al., Chem. Engin. J. 394 (2020) 125014.
[30] X. Tang, J. Chen, Y. Li, et al., Chem. Engin. J. 118 (2006) 119–125.
[31] J. Zhang, Y. Li, L. Wang, C. Zhang, H. He, Catal. Sci. Technol. 5 (2015) 2305–2313.
[32] L. Miao, Y.F. Xie, Y.T. Xia, N. Zou, J.L. Wang, Appl. Surf. Sci. 481 (2019) 404–413.
[33] K. Jiang, J. Zhang, Y. Wan, Z. Liu, J. Chen, Opt. Mater. 114 (2021) 110913.
[34] J. Li, D. Ren, Z. Wu, et al., J. Colloid Interf. Sci. 530 (2018) 78–87.
[35] J.L. Wang, J.E. Li, C.J. Jiang, et al., Appl. Catal. B: Environ. 204 (2017) 147–155.
[36] M. Chen, H.H. Wang, X.Y. Chen, et al., Chem. Engin. J. 390 (2020) 124481.
[37] L. Miao, Y. Xie, Y. Xia, N. Zou, J. Wang, Appl. Surf. Sci. 481 (2019) 404–413.
[38] R.M. Fang, H.B. Huang, J. Ji, et al., Chem. Engin. J. 334 (2018) 2050–2057.
[39] J.L. Wang, G.K. Zhang, P.Y. Zhang, J. Mater. Chem. A 5 (2017) 5719–5725.
[40] C. Wang, X.H. Zou, H.B. Liu, et al., Appl. Surf. Sci. 486 (2019) 420–430.
[41] J. Ji, X.L. Lu, C. Chen, M. He, H.B. Huang, Appl. Catal. B: Environ. 260 (2020) 118210.